Loading system for wind turbine drivetrain test bench with model-based compensation control strategy

Danyang Li [a], Yajing Gu*[a, b], Yonggang Lin [a, b], Jiajun Song [a], Xiangheng Feng [a], Hongwei Liu [a, b]

a. The State Key Laboratory of Fluid Power and Mechatronic Systems, Zhejiang University, Hangzhou, China

b. Ocean Academy, Zhejiang University, Zhoushan, China

danyang.li@zju.edu.cn, guyj90@zju.edu.cn, yglin@zju.edu.cn, jjsong07@zju.edu.cn, Xiangheng_f97@zju.edu.cn, lhwei@zju.edu.cn

Abstract.

The dramatic expansion of wind turbines sets higher demands on the drivetrain test bench. The loading system of the drivetrain test bench should accurately reproduce real wind loads on the ground to evaluate the reliability of turbine components. In this paper, the multi-cylinder electrohydraulic digital-servo loading technology is applied to the non-torque loading system. The hydraulic cylinders groups are designed to substitute the original loading points. The loading center of each cylinders group is deviated due to the installation distance and the changed force distribution. Thus, a novel loading principle is proposed to compensate for the eccentric moment. The loading formula should be recalculated in real-time to ensure the implementation of accurate reproduction of 5-DOF loads based on the integration of multiple hydraulic cylinders groups. In addition, there are reverse sudden changes caused by the asynchronous opening and closing characteristics of the servo valve and the onoff valve. An advanced model-based sliding mode controller compensation strategy is proposed to achieve smooth switching. A mathematical analytical model is derived to deal with the parametric uncertainties and nonlinearities. Moreover, the extensive AMESim-Simulink co-simulations under various signals that represent the real wind loads have been conducted to investigate the performance of the proposed control strategy. By comparing the advanced controller to a traditional PID controller, the simulation results showed that the switching error was greatly reduced and the total loading process was smoother for the model-based sliding mode controller compensation strategy. The excellent tracking performance proved the feasibility and effectiveness of the proposed strategy.

Keywords. Loading system, drivetrain test bench, model-based compensation control strategy, co-simulation.

1. INTRODUCTION

The development of large scale wind turbines has expanded dramatically during the past few decades with the global cumulative wind power capacity reaching 743 gigawatts (GW) by the end of 2020 **Errore. L'origine riferimento non è stata trovata.**. The research trend for the further development of wind power technology has been generalized to large offshore wind turbines above 15 megawatts (MW). The rapid growth of wind turbine capacity sets higher demands for the ground test and evaluation of components, including hardware components-structural, mechanical, electrical, thermal, hydraulic and software components **Errore. L'origine riferimento non è stata trovata.**. Unexpected failures of the drivetrain system, as the fundamental type of failure, require long waiting periods and higher maintenance costs **Errore. L'origine riferimento non è stata trovata.**. Thus, it is inevitable to implement a loading system for the wind turbine drivetrain test bench to identify evaluation issues and assess component performances.

The wind turbine is usually subjected to various loads, consisting of gravitational loads, aerodynamic loads and centrifugal loads **Errore. L'origine riferimento non è stata trovata.**. These loads compose of six-degree-of-freedom (6-DOF) loading elements including three moment elements and three force elements **Errore. L'origine riferimento non è stata trovata.**. The loading system should accurately reproduce real wind loads on the ground to evaluate the reliability of turbine components. There are several utility-scale drivetrain test benches worldwide. Fig. 1.1(a) shows the 4MW wind turbine system test bench at the Center for Wind Power Drives of RWTH Aachen University **Errore. L'origine riferimento non è stata trovata.**. Fig. 1.1(b) represents the 7.5 MW mechanical test benches conducted at the Wind Turbine Drivetrain Testing Facility at Clemson University **Errore. L'origine riferimento non è stata trovata.**. Fig. 1.1(c) depicts the 15 MW wind turbine nacelle test facility in Offshore Renewable Energy (ORE) Catapult **Errore. L'origine riferimento non è stata trovata.**. Fig. 1.1(d) illustrates the 25 MW test facility model which is the wind industry's largest and most advanced test bench in LORC **Errore. L'origine riferimento non è stata trovata.**.

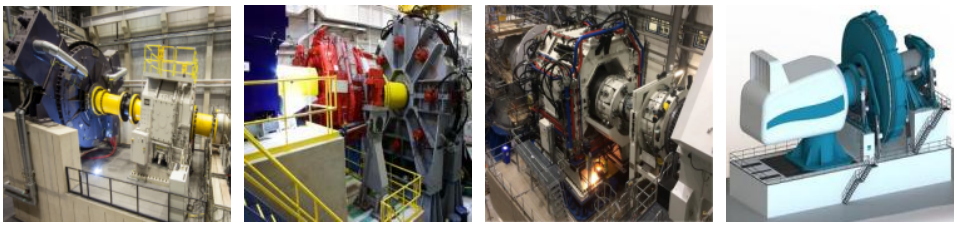

(a) (b) (c) (d)

Fig. 1.1 Photographs of wind turbine drivetrain test bench. (a) 4 MW test bench in RWTH Aachen University, (b)7.5 MW test bench in Clemson University, (c)15 MW test facility in ORE Catapult, (d) 25 MW test facility illustration in LORC.

The drivetrain test bench consists of the drive motor, the non-torque load unit and the device under test. The drive motor is able to emulate the wind torque loads. The other 5-DOF loads are reproduced by the non-torque load unit. A grid emulator can be mounted with the device under test and applied to a typical grid faults test. The critical research lies in the reproduction technology of non-torque loads. The non-torque loading system is composed of multiple

electrohydraulic actuators in various arrangements. The basic loading unit is an electrohydraulic servo valve and a hydraulic cylinder. However, with the dramatically increasing capacity of wind turbines, the loading force exerted by each servo-valve controlled (SVC) cylinder is growing. A novel multi-cylinder electrohydraulic digital-servo loading (MEDSL) is proposed to solve the inaccuracy loading problem for large load reproduction. A traditional single cylinder is replaced by a new hydraulic cylinders group that includes N hydraulic cylinders at each point, in which one is controlled by the electrohydraulic servo valve and the others (N-1) are controlled by the onoff valve **Errore. L'origine riferimento non è stata trovata.**. The loading accuracy is substantially increased. However, there are reverse sudden changes caused by the asynchronous opening and closing of the servo valve and the onoff valve. At the same time, the loading center of each cylinders group is deviated due to the installation distance and the changed force distribution. The above matters require an advanced controller to achieve the accurate reproduction of real wind loads.

As the increment of hydraulic cylinders, the control strategy turns to be more complex with more variables induced in the loading system. Many nonlinear controllers have been proposed for the multi-input multi-output (MIMO) system. The model-based control techniques can be employed to deal with the parametric uncertainties and nonlinearities of electrohydraulic systems. The necessary conditions for the feasibility of the MIMO sliding mode controller (SMC) were investigated **Errore. L'origine riferimento non è stata trovata.**. A nonlinear MIMO SMC was designed for tracking the pitch angle and the plunge of the wind turbine blade tip **Errore. L'origine riferimento non è stata trovata.**. The continuous SMC was proposed to ensure arbitrarily small errors as desired for a class of nonlinear MIMO systems **Errore. L'origine riferimento non è stata trovata.**. Samir Zeghlache *et al.* proposed an observer-based robust controller for two twin-rotor MIMO systems **Errore. L'origine riferimento non è stata trovata.**. Farzaneh Bagheri *et al.* proposes a MIMO SMC synchronizing the control of all state variables for the quasi-Z-source inverter feeding a load **Errore. L'origine riferimento non è stata trovata.**. The model-based control strategy can effectively deal with the nonlinear issues and realize precise control effects based on adaptive and robust control theory. Therefore, in this paper, a model-based compensation control strategy was proposed for the MEDSL system. The loading performance was investigated by the AMESim and Simulink co-simulation. The results showed the advantages of the controller. It builds a foundation for the non-torque loading system of MW-class wind turbines.

This paper is organized as follows. The modified loading scheme of MEDSL is constructed considering the eccentric moment of hydraulic cylinders in Section II. The mathematical analytical model of MEDSL is derived and the model-based compensation controller is designed in Section III. In Section IV, the effect of the proposed control strategy is studied based on the co-simulation platform. Section V discusses the conclusion and future work.

2. LOADING SCHEMES

The real rotor and blades are substituted by a rotating loading disc. The mass and inertia moment is designed as the equivalent of the real wind turbine components. The distribution of hydraulic cylinders employs symmetrical loading scheme. Eight axial electrohydraulic loading points are symmetrically positioned on each left and right side of the disc. Eight radial

loading points are evenly distributed on the circumferential surface of the disc. Each loading point is composed of a digital-servo hydraulic cylinders group, including an SVC cylinder and (N-1) onoff valve controlled (OVC) cylinder. The loading force of each cylinders group can be defined as

$$F_{Li} = F_{Li0} + \sum_{n=1}^{N-1} F_{Lin} \tag{2.1}$$

$$F_{Ri} = F_{Ri0} + \sum_{n=1}^{N-1} F_{Rin} \tag{2.2}$$

$$F_{di} = F_{di0} + \sum_{n=1}^{N-1} F_{din} \tag{2.3}$$

$$F_{d'i} = F_{d'i0} + \sum_{n=1}^{N-1} F_{d'in} \tag{2.4}$$

where F_{Li} (i=1~8) denotes the loading force of the left side of the loading disc; F_{Li0} is the loading force of the SVC cylinder; F_{Lin} represents the loading force of the OVC cylinder; N is the number of cylinders in a group; F_{Ri} (i=1~8)denotes the loading force of the right side of the loading disc; F_{di} and $F_{d'i}$ (i=1~4) are the loading force of radial surface of the disc, as shown in Fig. 2.1, which illustrates the N=4 case.

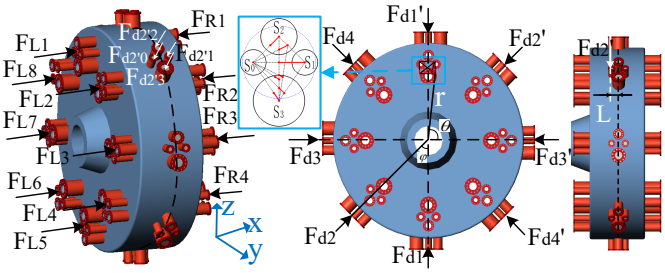

Figure 2.1. Loading diagram and the distribution of the loading vectors

The force of one loading point and its symmetrical counterpart can be considered as a loading force unit. The axial loading force F_{Ai} and the radial loading force F_{ri} can be expressed as

$$F_{Ai} = F_{Li} - F_{Ri} \quad (i = 1 \sim 8) \tag{2.5}$$

$$F_{ri} = F_{di} - F_{di'} \quad (i = 1 \sim 4) \tag{2.6}$$

However, there exists an eccentric moment due to the installation distance and the changed force distribution of the cylinders group. As can be seen from the blue box in Fig. 2.1, the central loading point of each hydraulic cylinders group is a factor varying with the change of the loading force. Thus, the loading radius, the eccentricity and the angle with the coordinate axis are all variables. Hence, the loading force vectors and the load vectors can be defined as

$$\mathbf{F} = \left[F_{A1}, F_{A2}, F_{A3}, F_{A4}, F_{A5}, F_{A6}, F_{A7}, F_{A8}, F_{R1}, F_{R2}, F_{R3}, F_{R4}\right]^{\mathrm{T}} \tag{2.7}$$

$$\mathbf{W} = \left[F_x, F_y, F_z, M_y, M_z\right]^{\mathrm{T}} \tag{2.8}$$

The balance equation between the force vectors and the load vectors is governed as

$$\begin{bmatrix} F_x \\ F_y \\ F_z \\ M_y \\ M_z \end{bmatrix} = \begin{bmatrix} 1 & 1 & 1 & 1 & 1 & 1 & 1 & 1 & 0 & 0 & 0 & 0 \\ 0 & 0 & 0 & 0 & 0 & 0 & 0 & 0 & \sin\phi_1 & \sin\phi_2 & \sin\phi_3 & \sin\phi_4 \\ 0 & 0 & 0 & 0 & 0 & 0 & 0 & 0 & \cos\phi_1 & \cos\phi_2 & \cos\phi_3 & \cos\phi_4 \\ r_1\sin\theta_1 & r_2\sin\theta_2 & r_3\sin\theta_3 & r_4\sin\theta_4 & r_5\sin\theta_5 & r_6\sin\theta_6 & r_7\sin\theta_7 & r_8\sin\theta_8 & L_1\cos\phi_1 & L_2\cos\phi_2 & L_3\cos\phi_3 & L_4\cos\phi_4 \\ r_1\cos\theta_1 & r_2\cos\theta_2 & r_3\cos\theta_3 & r_4\cos\theta_4 & r_5\cos\theta_5 & r_6\cos\theta_6 & r_7\cos\theta_7 & r_8\cos\theta_8 & L_1\sin\phi_1 & L_2\sin\phi_2 & L_3\sin\phi_3 & L_4\sin\phi_4 \end{bmatrix} \bullet \begin{bmatrix} F_{A1} \\ F_{A2} \\ F_{A3} \\ F_{A4} \\ F_{A5} \\ F_{A6} \\ F_{A7} \\ F_{A8} \\ F_{R1} \\ F_{R2} \\ F_{R3} \\ F_{R4} \end{bmatrix} \tag{2.9}$$

where r_i (i=1~8) is the distance between the actual loading point of each cylinders group and the center of the loading disk; θ_i (i=1~8)denotes the angle between the actual loading point of each axial cylinders group and the positive direction of the y-axis; L_i (i=1~4) represents the distance between the actual loading point of each radial cylinders group and the radial centerline of the circumferential surface of the loading disc; φ_i (i=1~4) is the angle between the actual loading point of each radial cylinders group and the negative direction of the z-axis.

Equation (2.9) can be solved as

$$\mathbf{W} = \mathbf{P} \bullet \mathbf{F} \Leftrightarrow \mathbf{F} = \mathbf{P}^{-1} \bullet \mathbf{W} \tag{2.10}$$

where **W** denotes the load vectors; **F** is the loading force vectors; **P** is the transformation matrix between the total load vectors and the loading force vectors; $\mathbf{p}^{-1}$ is the inverse transformation matrix of **P**. The matrix **P** can be written as

$$\mathbf{p} = \begin{bmatrix} 1 & 1 & 1 & 1 & 1 & 1 & 1 & 1 & 0 & 0 & 0 & 0 \\ 0 & 0 & 0 & 0 & 0 & 0 & 0 & 0 & \sin\phi_1 & \sin\phi_2 & \sin\phi_3 & \sin\phi_4 \\ 0 & 0 & 0 & 0 & 0 & 0 & 0 & 0 & \cos\phi_1 & \cos\phi_2 & \cos\phi_3 & \cos\phi_4 \\ r_1\sin\theta_1 & r_2\sin\theta_2 & r_3\sin\theta_3 & r_4\sin\theta_4 & r_5\sin\theta_5 & r_6\sin\theta_6 & r_7\sin\theta_7 & r_8\sin\theta_8 & L_1\cos\phi_1 & L_2\cos\phi_2 & L_3\cos\phi_3 & L_4\cos\phi_4 \\ r_1\cos\theta_1 & r_2\cos\theta_2 & r_3\cos\theta_3 & r_4\cos\theta_4 & r_5\cos\theta_5 & r_6\cos\theta_6 & r_7\cos\theta_7 & r_8\cos\theta_8 & L_1\sin\phi_1 & L_2\sin\phi_2 & L_3\sin\phi_3 & L_4\sin\phi_4 \end{bmatrix} \tag{2.11}$$

Therefore, the loading force vector **F** can be solved using (2.7)-(2.11). The loading formula should be recalculated in real-time to ensure the implementation of accurate reproduction of 5-DOF loads based on the integration of multiple hydraulic cylinders groups.

3. CONTROLLER DEVELOPMENT

The accuracy of the loading system with MEDSL depends on each cylinders group. However, the response speed of the SVC cylinder is faster than the OVC cylinder. Thus, there are reverse sudden changes in each switching process. To compensate for this loading error, a model-based SMC control strategy is proposed. The condition of an SVC cylinder and an OVC cylinder is investigated.

3.1. State-space Modelling

The load flow rate model of SVC and OVC cylinders can be depicted as **Errore. L'origine riferimento non è stata trovata.**

$$Q_{Ls} = A_s \frac{dx_s}{dt} + C_{tps} p_{Ls} + \frac{V_s}{4\beta_{es}} \frac{dp_{Ls}}{dt} \tag{3.1}$$

$$Q_{Lo} = A_o \frac{dx_o}{dt} + C_{tpo} p_{Lo} + \frac{V_o}{4\beta_{eo}} \frac{dp_{Lo}}{dt} \tag{3.2}$$

where Q_{Ls} and Q_{Lo} are the flow of the servo-valve and the onoff valve; A_s and A_o are the effective area of the piston for SVC and OVC cylinder; x_s and x_o are defined as the spool displacement of the servo-valve and the onoff valve; C_{tps} and C_{tpo} are the total leakage coefficient of the SVC and OVC cylinder; p_{Ls} and p_{Lo} are the load pressure of the SVC and OVC cylinder; β_{es} and β_{eo} are the oil effective bulk modulus; V_s and V_o are the total volume of the SVC and OVC cylinder. The force balance equation of the hydraulic cylinder is

$$A_s p_{Ls} = m_s \frac{d^2 x_s}{dt^2} + B_s \frac{dx_s}{dt} + K_s x_s \tag{3.3}$$

$$A_o p_{Lo} = m_o \frac{d^2 x_o}{dt^2} + B_o \frac{dx_o}{dt} + K_o x_o \tag{3.4}$$

where m_s and m_o are the equivalent mass; B_s and B_o are the equivalent viscous damping coefficient; K_s and K_o are the load spring stiffness of SVC and OVC cylinder, respectively. The relationship between the input control signal and the spool displacement can be described as

$$x_s = \frac{k_s}{\tau_s + 1} u_s \tag{3.5}$$

$$x_o = \frac{k_o}{\tau_o + 1} u_o \tag{3.6}$$

where k_s and τ_s denotes the gain and the time constant of the first-order inertia element for the servo valve; k_o and τ_o denotes the gain and the time constant of the first-order inertia element for the onoff valve; u_s and u_o are the input signal of servo valve and the onoff valve, respectively. The pressure-flow characteristic equation of the servo valve and the onoff valve can be written as

$$Q_{Ls} = \frac{k_{sz}}{\tau_s + 1} g(u_s) u_s \quad g(u_s) = \sqrt{p_s - \mathrm{sgn}(u_s) p_{Ls}} \tag{3.7}$$

$$Q_{Lo} = \frac{k_{oz}}{\tau_o + 1} g(u_o) u_o \quad g(u_o) = \sqrt{p_s - \mathrm{sgn}(u_o) p_{Lo}} \tag{3.8}$$

where k_{sz} and k_{oz} are the coefficient of servo-valve and onoff valve, and p_s denotes the pressure of the system. Define a set of state variables as

$$x=\left[x_1,x_2,x_3,x_4,x_5,x_6,x_7,x_8,y\right]^T=\left[x_s,\dot{x}_s,p_{Ls},\dot{p}_{Ls},x_o,\dot{x}_o,p_{Lo},\dot{p}_{Lo},y\right]^T \tag{3.9}$$

where y is the total loading force of the system. The state-space model can be described as

$$\begin{aligned}
&\dot{x}_1=x_2\\
&\dot{x}_2=-a_1x_1-a_2x_2+a_3x_3\\
&\dot{x}_3=x_4\\
&\dot{x}_4=\frac{1}{\tau_s}\left[-a_6x_1-a_7x_2-a_8x_3-a_9x_4+b_1k_{sz}g(u_s)u_s\right]\\
&\dot{x}_5=x_6\\
&\dot{x}_6=-a_{11}x_5-a_{12}x_6+a_{13}x_7\\
&\dot{x}_7=x_8\\
&\dot{x}_8=\frac{1}{\tau_{o1}}\left[-a_{16}x_5-a_{17}x_6-a_{18}x_7-a_{19}x_8+b_2k_{oz}g(u_o)u_o\right]\\
&y=x_3A_s+x_7A_o
\end{aligned} \tag{3.10}$$

where $a_1=k_s/m_s$, $a_2=B_s/m_s$, $a_3=A_s/m_s$, $a_4=4\beta_{es}A_s/V_s$, $a_5=4\beta_{es}C_{tps}/V_s$, $b_1=4\beta_{es}/V_s$, $a_6=-a_1a_4\tau_s$, $a_7=a_4-a_2a_4\tau_s$, $a_8=a_5+a_3a_4\tau_s$, $a_9=a_5\tau_s+1$, $a_{11}=k_o/m_o$, $a_{12}=B_o/m_o$, $a_{13}=A_o/m_o$, $a_{14}=4\beta_{eo}A_o/V_o$, $a_{15}=4\beta_{eo}C_{tpo}/V_o$, $b_2=4\beta_{eo}/V_o$, $a_{16}=-a_{11}a_{14}\tau_o$, $a_{17}=a_{14}-a_{12}a_{14}\tau_o$, $a_{18}=a_{15}+a_{13}a_{14}\tau_o$, $a_{19}=a_{15}\tau_o+1$.

3.2. Model-based SMC Design

Set y_d as the expected total loading force of the system, and the tracking error and its derivatives are given by

$$\begin{cases}e_1=y_d-y\\ e_2=\dot{y}_d-\dot{y}\\ e_3=\ddot{y}_d-\ddot{y}\end{cases} \tag{3.11}$$

Design the sliding mode switching function of the system as

$$s=c_1e_1+c_2e_2 \tag{3.12}$$

where c_1 and c_2 are the positive coefficients of the switching function. The derivative of the switching function is given by

$$\dot{s}=c_1e_2+c_2e_3 \tag{3.13}$$

The reaching law is chosen as depicted to obtain SMC

$$\dot{s}=-\varepsilon\mathrm{sat}(\frac{s}{\phi})-ks \tag{3.14}$$

where ε, k are both positive real parameters, ϕ is the thickness of the boundary layer. And the saturation function is defined as follows to eliminate the chattering problem

$$\mathrm{sat}(\frac{s}{\phi})=\begin{cases}\dfrac{s}{\phi} & \text{if}\left|\dfrac{s}{\phi}\right|<1,\\ \mathrm{sgn}(\dfrac{s}{\phi}) & \text{if}\left|\dfrac{s}{\phi}\right|\geq 1,\end{cases} \tag{3.15}$$

The expression of the model-based SMC strategy can be obtained

$$a_{10}g(u_s)u_s + a_{20}g(u_o)u_o = (c_1e_2 + \varepsilon sat(\frac{s}{\varphi}) + ks) / c_2 + \ddot{y}d - \left(A_s f_s(x) + A_o f_o(x)\right) \quad (3.16)$$

where $a_{10} = A_s b_1 k_{sz} / \tau_s, a_{20} = A_o b_2 k_{oz} / \tau_o, f_s(x) = (-a_6 x_1 - a_7 x_2 - a_8 x_3 - a_9 x_4) / \tau_s,$ $f_o(x) = \left(-a_{16} x_5 - a_{17} x_6 - a_{18} x_7 - a_{19} x_8\right) / \tau_o.$

4. SIMULATION RESEARCH

A co-simulation model of the one SVC cylinder and one OVC cylinder case has been built in AMESim and Simulink to validate the effect of the model-based SMC compensation control strategy. The details of the simulation are listed in Table I. The other related parameters are set as the default values in AMESim. As shown in Fig. 3.1(a), the hydraulic model consists of the motor, the relief valve, the three-position four-way servo valve, the two-position four-way solenoid directional valve, two identical hydraulic cylinders, the equivalent load and the co-simulation interface. The model-based SMC compensation strategy is calculated in Simulink as illustrated in Fig. 3.1(b). The simulation step is 1e-4 s, and the total simulation time is 10 s.

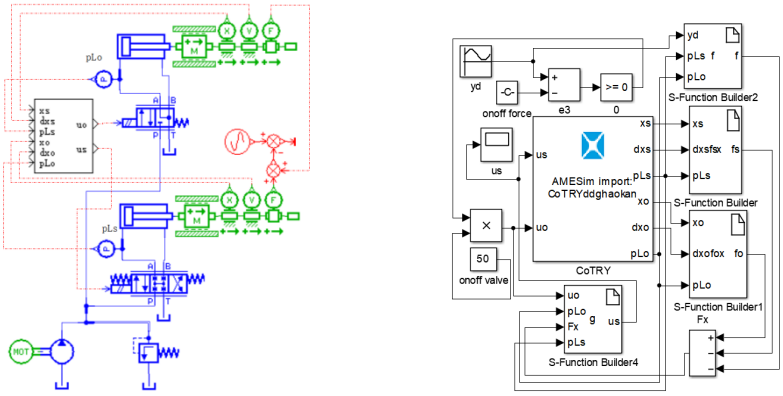

(a) (b)

Fig. 3.1 Co-simulation model in AMESim and Simulink.

To investigate the performance of the model-based SMC compensation method, the traditional proportional-integral-derivative (PID) controller was used to be compared under various sinusoidal signals. The first simulation was carried out using 0.2 Hz sinusoidal total loading wave. As illustrated in Fig. 3.2(a), the total loading force of the system is the sum of loading forces from the SVC cylinder and OVC cylinders. The maximum force that can be exerted by the SVC cylinder was about 10 kN. Thus, the force was increasing stably before 1.25 s. The input signal of the OVC cylinder was a series of digital values. Then the OVC cylinder was open to offer the maximum force while the force of the SVC cylinder is 0 at this time.

TABLE 3.1 SIMULATION PARAMETERS

Component	Parameter	Value	Component	Parameter	Value

hydraulic cylinder	Piston diameter /mm	50	Hydraulic source	Pressure source /MPa	5
	Rod diameter /mm	32		Pump displacement (cc /rev)	100
	Cylinder stroke /mm	50		Typical speed of pump (rev/min)	1500
	Bulk modulus /MPa	800	SMC	c_1	5e3
				c_2	10
	Leakage coefficient	2e-13	SMC	ε	1e4
				k	500
	τ_s	1.25e-3		ϕ	1e-3
	τ_o	8e-3	PID	P	0.9
	k_{sz}	1.36e-10		I	0.5
	k_{oz}	2.46e-10		D	0.008

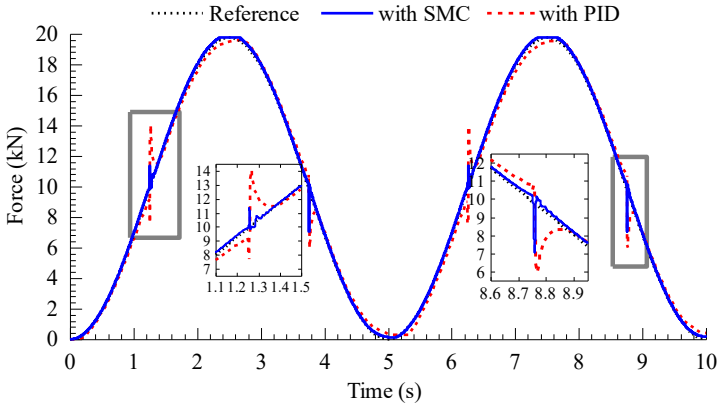

(a)

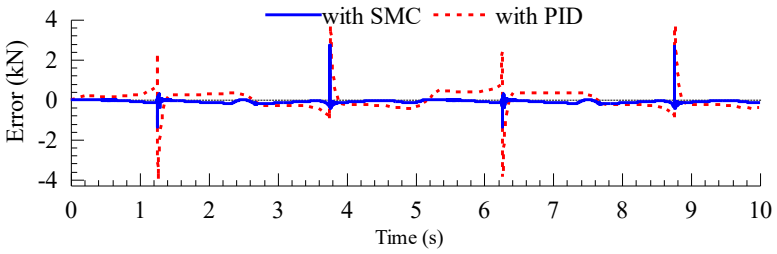

(b)

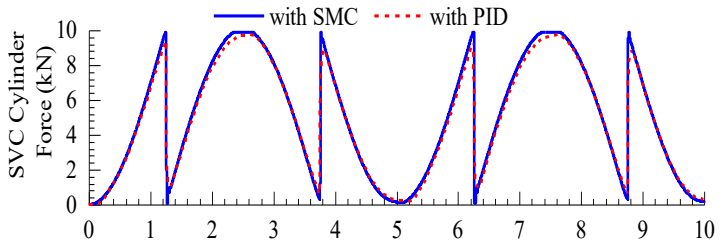

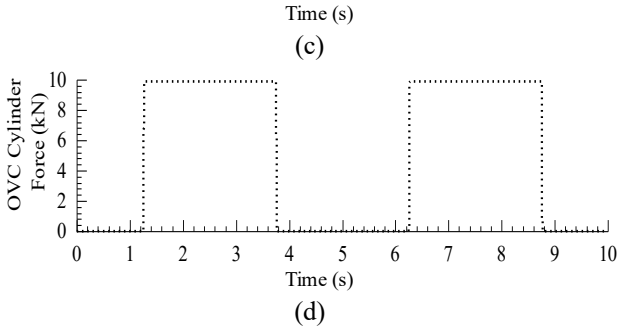

Fig. 3.2 Simulation results for 0.2 Hz loads. (a) Tracking performance. (b) Tracking error. (c) Tracking force of SVC cylinder. (d) Tracking force of OVC cylinder.

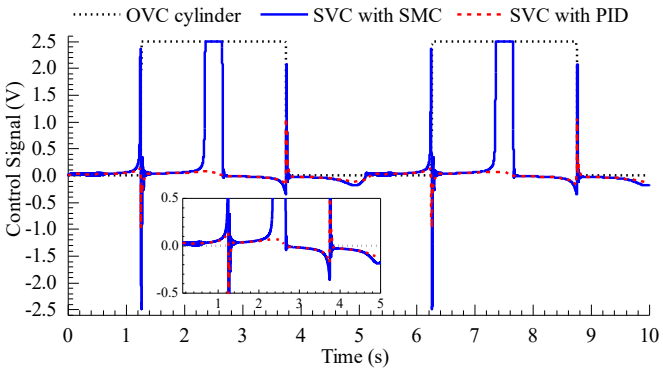

Fig. 3.3 Simulation results for control signal of 0.2 Hz loading.

As can be seen from Fig. 3.2(a), the total loading force had an obvious trend of increasing first and then reducing for the PID controller. A similar phenomenon appeared in the decreasing process. However, the model-based SMC compensation strategy exhibited better tracking performance by considering the asynchronous opening and closing characteristics of the servo valve and the onoff valve. The control signals was shown in Fig. 3.3, the input signal of OVC cylinder was a series of square wave, the input signal of SVC cylinder had impulse response at switching.

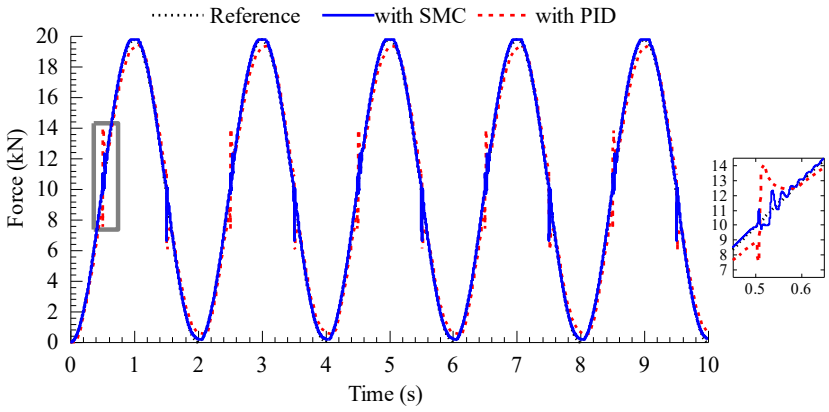

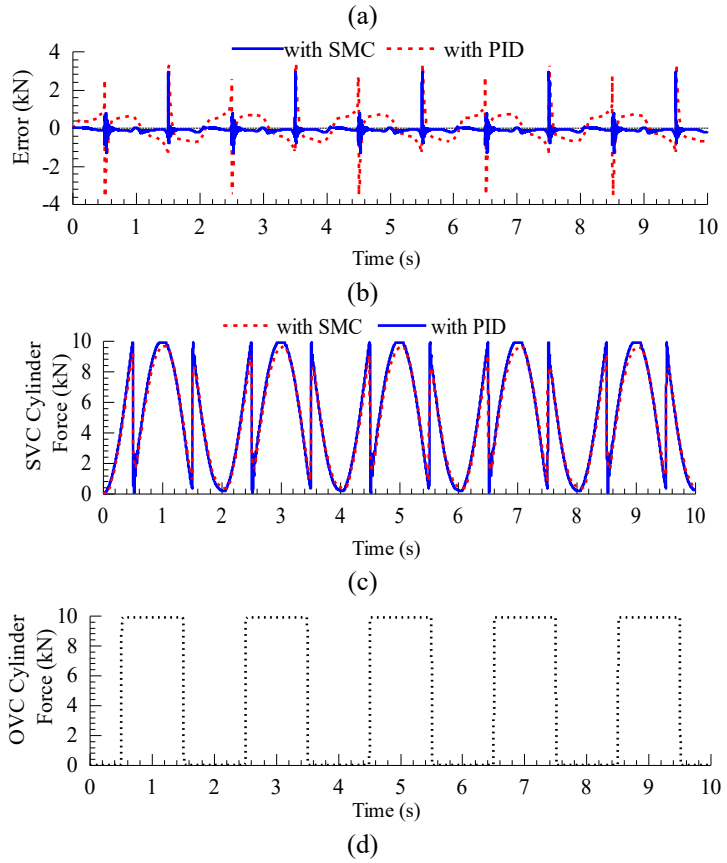

Fig. 3.4 Simulation results for 0.5 Hz loads. (a) Tracking performance. (b) Tracking error. (c) Tracking force of the SVC cylinder. (d) Tracking force of the OVC cylinder.

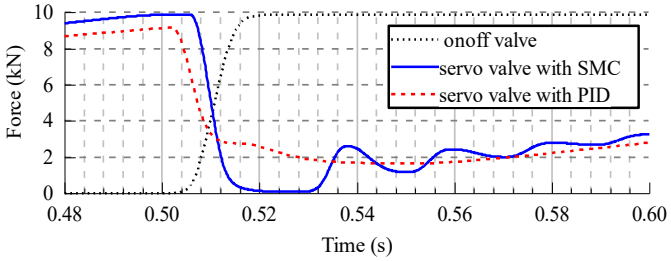

Fig. 3.5 Simulation results for the 0.5 s switching time of the servo valve and onoff valve.

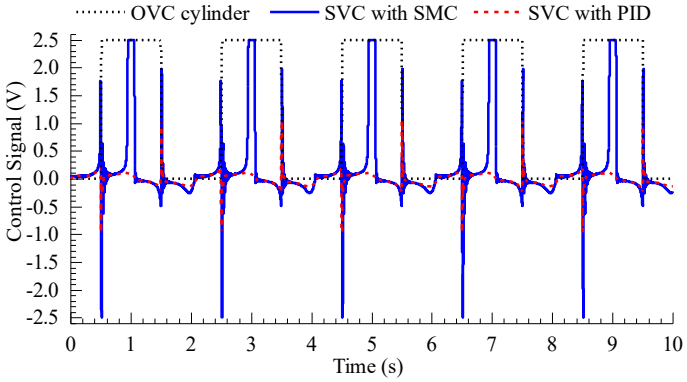

Fig. 3.6 Simulation results for the control signal of 0.5 Hz loading.

Moreover, the effect of the model-based SMC compensation strategy was also tested for 0.5 Hz and 1 Hz sinusoidal loads, as shown in Fig. 3.4 and Fig. 3.7, respectively. And the control signals for 0.5 Hz and 1 Hz sinusoidal loads of the servo valve and the onoff valve were shown in Fig. 3.6 and Fig. 3.8, respectively. It can be seen from the enlarged figure of Fig. 3.4(a), the switching error is reduced from about 6.3 kN to 2.4 kN at 0.5 s switching time. By expanding the simulation result of the switching process as plotted in Fig. 3.5, the response time of the onoff valve was about 20 ms while the servo valve began to respond in 3 ms under the PID controller. Thus, the total loading force declined rapidly and then rebounded with the onoff valve gradually opening. In contrast, the servo valve under model-based SMC actively slowed down the response speed. It began to respond in 9 ms. Therefore, the total loading force was relatively increasing smoothly. Besides, the tracking error except for the switching error was within 0.4 kN for SMC while the tracking error was about 1.4 kN for PID control as shown in Fig. 3.7(b). It can be concluded that the switching error is greatly reduced and the tracking performance is better for the model-based SMC compensation strategy.

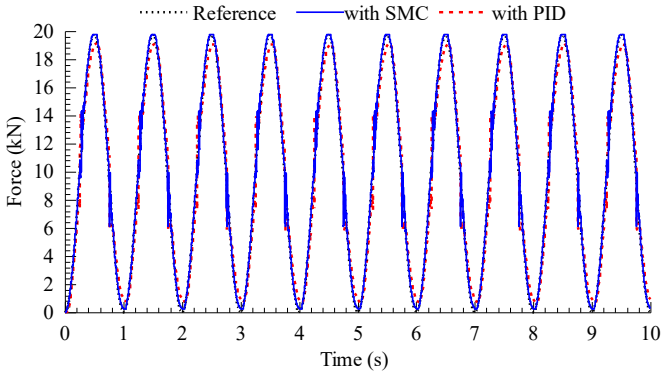

(a)

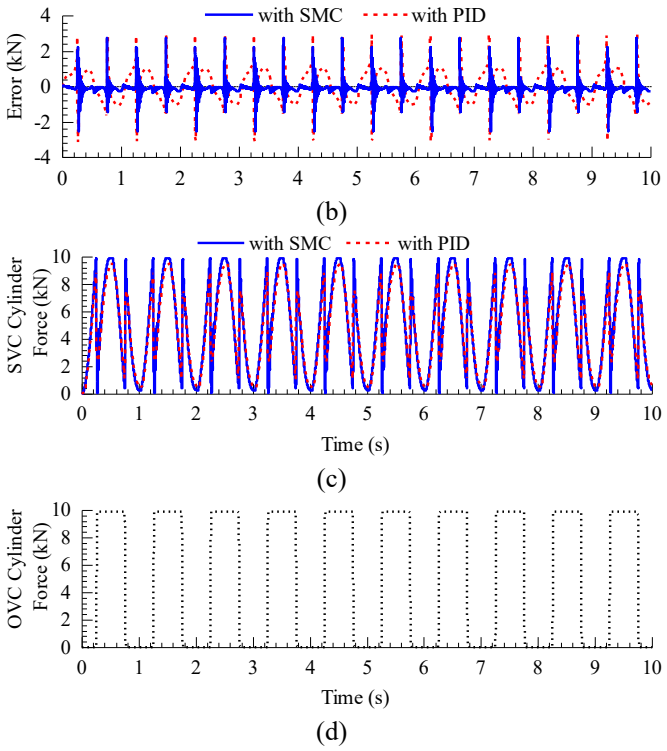

Fig. 3.7 Simulation results for 1.0 Hz loads. (a) Tracking performance. (b) Tracking error. (c) Tracking force of the SVC cylinder. (d) Tracking force of the OVC cylinder.

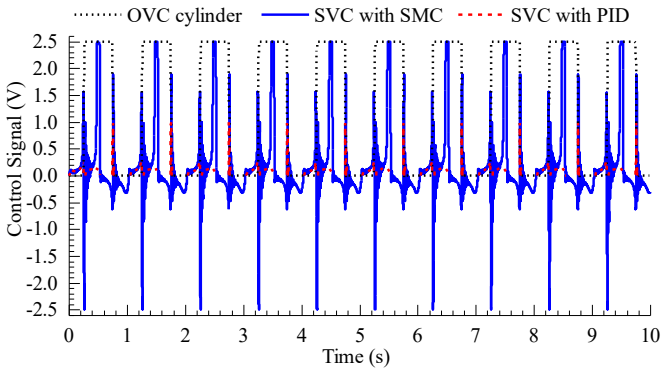

Fig. 3.8 Simulation results for the control signal of 1 Hz loading.

5. CONCLUSION

In this paper, the method of applying MEDSL to the non-torque hydraulic loading system is proposed. To solve the eccentric moment caused by the installation distance and the changed force distribution, the whole loading principle is designed. The loading formula is set up to ensure the implementation of accurate reproduction of 5 DOF loads. In addition, a model-based SMC compensation control strategy is proposed aiming at the asynchronous switching

characteristic of the servo valve and the onoff valve. The loading performance is investigated by the AMESim and Simulink co-simulation. The results show that the switching error is reduced and the total loading process is smoother by using the advanced controller.

Furthermore, for the total loading force, the switching error of the descending process is larger than that of the ascending process. This is mainly due to the difference between opening and closing characteristics, which should be solved in further research. Besides, this paper shows the control strategy of one servo valve and one onoff valve condition, which is the foundation theory of the MEDSL system. The extended cases for more OVC cylinder are not considered and illustrated which can be explored in further studies. Moreover, the research of twelve force application points, involving additional disturbances and accurate calculation of loading matrix, will be the focus research of the next stage for the author's work.

6. ACKNOWLEDGMENT

This study was supported in part by the National Key R&D Program of China under Grant 2018YFB1501900, in part by the Science Fund for Creative Research Groups of National Natural Science Foundation of China under Grant 51821093, in part by the Youth Foundation of National Natural Science Foundation of China under Grant 51905472, and in part by Zhejiang Provincial Natural Science Foundation of China under Grant LZ19E050001.

7. REFERENCES

[1] Global Wind Energy Council, Global Wind Report 2021 [Online]. Available: https://gwec.net/global-wind-report-2021/.

[2] J. M. P. Pérez, F. P. G. Márquez, A. Tobias, M. Papaelias, "Wind turbine reliability analysis," Renewable Sustain. Energy Rev., vol. 23, pp. 463-472, 2013.

[3] K. Y. Oh, J. K. Lee, H. J. Bang, J.Y. Park, J. S. Lee, B. I. Epureanu, "Development of a 20 kW wind turbine simulator with similarities to a 3 MW wind turbine," Renewable Energy, vol. 62, pp. 379-387, 2014.

[4] X. Yin, Y. Lin, W. Li, H. Ye, "Loading system and control strategy for simulating wind turbine loads," J. Vib. Control, vol. 23, no. 11, pp. 1739-1752, 2015.

[5] X. Yin, Y. Lin, W. Li, H. Ye, Y. Gu, and H. Liu, "Reproduction of five degree-of-freedom loads for wind turbine using equispaced electro-hydraulic actuators," Renewable Energy, vol. 83, pp. 626-637, 2015.

[6] N. Averous, M. Stieneker, S. Kock, C. Andrei, A. Helmedag, R. De Doncker, et al., "Development of a 4 MW full-Size wind-turbine test bench," IEEE Trans. Emerg. Sel. Topics Power Electron., vol. 5, no. 2, pp. 600-609, 2017.

[7] R. F. Schkoda, "Sliding mode control of a hydraulically actuated load application unit with application to wind turbine drivetrain testing," IEEE Trans. Control Syst. Technol., vol. 23, no. 6, pp. 2203-2215, 2015.

[8] Offshorre Renewable Energy, Powertrain Testing Services [Online]. Available: https://ore.catapult.org.uk/what-we-do/testing-validation%e2%80%a8/powertrain-facilities/.

[9] R&D, R&D Test Systems is developing the world's largest test bench for LORC [Online]. Available: https://www.rd-as.com/insights/worlds-largest-test-bench-lorc/.

[10] Y. Lin, D. Li, Y. Gu, H. Liu, X. Feng, J. Ding, "Multi-cylinder electrohydraulic digital loading technology for reproduction of large load," Mechatronics, vol. 76, pp. 1-10, 2021.
[11] A. Palmieri, R. Procopio, A. Bonfiglio, M. Brignone, M. Invernizzi, A. Morini, B. Veselic, "Tuning and Feasibility Analysis of Classical First-Order MIMO Non-Linear Sliding Mode Control Design for Industrial Applications." Machines, vol. 7, no. 10, 2019.
[12] R. Agarwala, R. A. Chin, P. Malali, "Design of a nonlinear multi-input–multi-output sliding mode pitch angle and plunge controller for a 5MW wind turbine blade tip," Energy Sources, Part A: Recovery, Utilization, and Environmental Effects, 2019.
[13] H. Cho, T. Wanichanon, F.E. Udwadia, "Continuous sliding mode controllers for multi-input multi-output systems," Nonlinear Dyn., 2018.
[14] S. Zeghlache, N. Amardjia, "Real time implementation of nonlinear observer-based fuzzy sliding mode controller for a twin rotor multi-input multi-output system (TRMS)," Optik, vol. 156, pp. 391-407, 2018.
[15] F. Bagheri, H. Komurcugil, O. Kukrer, N. Guler, S. Bayhan, "Multi-Input Multi-Output-Based Sliding-Mode Controller for Single-Phase Quasi-Z-Source Inverters," IEEE Trans. Ind. Electron., vol. 67, no. 8, pp. 6439-6449, 2020.
[16] Y. Gu, Y. Lin, Q. Xu, H. Liu, W. Li, "Blade-pitch system for tidal current turbines with reduced variation pitch control strategy based on tidal current velocity preview," Renewable Energy, vol. 115, pp. 149-158, 2018.

Biographies

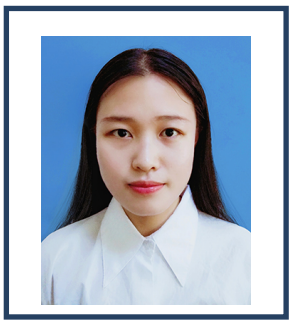

Danyang Li received the B.Eng degree from Yanshan University, Qinhuangdao, China, in 2019. She is currently working toward the Ph.D. degree in mechatronic engineering at Zhejiang University. Her research interests include the test system of wind turbine and electro-hydraulic system control.

Yajing Gu received the B.S. degree and the Ph.D. degree both in mechatronics from Zhejiang University, Hangzhou, China, in 2013 and 2018, respectively. He is currently a research associate at Zhejiang University. His research interests include ocean energy system, intelligent control, and multi-turbine array design.

Yonggang Lin received the M.Eng. degree from Jilin University, Changchun, China, in 2001, and the Ph.D. degree from Zhejiang University, Hangzhou, China, in 2005, both in mechatronic engineering.

In 2016, he was promoted to the rank of Professor at Zhejiang University. His research interests include machinery and electrohydraulic control of wind turbines, wave energy converters, and marine current turbines.

Jiajun Song received the B.S. degree from Beijing Institute of Technology, Beijing, China, in 2012, the M.Sc. and the Ph.D. degree from Michigan Technological University, Michigan, US, in 2020, all in Mechanical Engineering. In 2021, he started working as a post-doc in Zhejiang University. His research interests include wave energy converters, optimization algorithm, and optimal control.

Xiangheng Feng received B.Eng. Degree from Nanjing University of Aero-nautics and Astronautics, Nanjing, China, in 2019. He is currently working toward the Ph.D. degree in mechatronic engineering at Zhejiang University. His research interests include floating offshore wind turbine and load control system.

Hongwei Liu received the M.Eng. degree from the Taiyuan University of Technology, Taiyuan, China, in 2004, and the Ph.D. degree from Zhejiang University, Hangzhou, China, in 2009, both in mechatronic engineering. In 2011, he became a Faculty Member with Zhejiang University, where he was promoted to the rank of Associate Professor, in 2013. He is the Reviewer of Renewable and Sustainable Energy Reviews and Automation of Electric Power Systems. His research interests include ocean energy, hydraulic transmission system, and mechatronic system.